Radiotherapy and Oncology 140 (2019) 41–53

Contents lists available at ScienceDirect

Radiotherapy and Oncology

journal homepage: www.thegreenjournal.com

Review Article

Quantifying effects of radiotherapy-induced microvascular injury; review of established and emerging brain MRI techniques

Justyna Kłos [a,*], Peter Jan van Laar [b,c], Peter F. Sinnige [d], Roelien H. Enting [e], Miranda C.A. Kramer [d], Hiske L. van der Weide [d], Mark A. van Buchem [f], Rudi A.J.O. Dierckx [a], Ronald J.H. Borra [a], Anouk van der Hoorn [b,g]

[a] Department of Nuclear Medicine and Molecular Imaging; [b] Department of Radiology, Medical Imaging Center, University Medical Center Groningen, University of Groningen; [c] Department of Radiology, Zorggroep Twente, Almelo and Hengelo, SZ Almelo; [d] Department of Radiation Oncology; [e] Department of Neurology, University Medical Center Groningen, University of Groningen; [f] Department of Radiology, Leiden University Medical Center, The Netherlands; and [g] Brain Tumour Imaging Group, Division of Neurosurgery, Department of Clinical Neurosciences, University of Cambridge and Addenbrooke's Hospital, Cambridge, UK

ARTICLE INFO

Article history:
Received 26 February 2019
Received in revised form 16 May 2019
Accepted 17 May 2019
Available online 5 June 2019

Keywords:
Radiotherapy-induced injury
Susceptibility-weighted imaging (SWI)
Quantitative susceptibility mapping (QSM)
Dynamic susceptibility contrast MRI (DSC-MRI)
Cerebral microbleeds (CMB)
Microvascular

ABSTRACT

Microvascular changes are increasingly recognised not only as primary drivers of radiotherapy treatment response in brain tumours, but also as an important contributor to short- and long-term (cognitive) side effects arising from irradiation of otherwise healthy brain tissue. As overall survival of patients with brain tumours is increasing, monitoring long-term sequels of radiotherapy-induced microvascular changes in the context of their potential predictive power for outcome, such as cognitive disability, has become increasingly relevant. Ideally, radiotherapy-induced significant microvascular changes in otherwise healthy brain tissue should be identified as early as possible to facilitate adaptive radiotherapy and to proactively start treatment to minimise the influence on these side-effects on the final outcome.

Although MRI is already known to be able to detect significant long-term radiotherapy induced microvascular effects, more recently advanced MR imaging biomarkers reflecting microvascular integrity and function have been reported and might provide a more accurate and earlier detection of microvascular changes. However, the use and validation of both established and new techniques in the context of monitoring early and late radiotherapy-induced microvascular changes in both target-tissue and healthy tissue currently are minimal at best.

This review aims to summarise the performance and limitations of existing methods and future opportunities for detection and quantification of radiotherapy-induced microvascular changes, as well as the relation of these findings with key clinical parameters.

Novel therapies combined with molecular and genetic tumour biomarkers have enabled personalised brain cancer treatment, aiming to improve survival [1–5]. However, in patients with *low-grade brain tumours, with relatively long survival*, initial positive treatment responses are often overshadowed by negative long-term side effects of the treatment [6,7]. In order to minimise these effects, the whole therapeutic approach has become more and more oriented towards optimising the quality of remaining life and not only on treating the brain tumour itself [1,8]. With radiotherapy being a key component of the therapeutic approach, monitoring early signs of radiotherapy-induced injury related to irreversible clinical outcomes, such as cognitive dysfunction, has therefore become increasingly relevant.

The adverse effects of radiotherapy are believed to be related to microvascular endothelial injury, glial cell destruction and inflammation, with the synergistic interaction of these processes

Abbreviations: MRI, magnetic resonance imaging; T1, T1-weighted imaging; T2, T2-weighted imaging; FLAIR, fluid attenuated inversion recovery; DWI, diffusion-weighted imaging; DCE, dynamic contrast-enhanced; $T2^*$, $T2^*$-weighted gradient echo; SWI, susceptibility-weighted imaging; CMBs, cerebral microbleeds; WML, white matter lesions; QSM, quantitative susceptibility mapping; DSC, dynamic susceptibility contrast; VAI, vessel architectural imaging; ASL, arterial spin labelling; DTI, diffusion tensor imaging; IVIM, intravoxel incoherent motion; SRS, stereotactic radiosurgery; WBRT, whole brain radiotherapy; IQ, intelligence quotient; PBRT, proton beam radiation therapy; IMRT, intensity-modulated radiation therapy; RBE, relative biological effectiveness; CSF, cerebrospinal fluid; ADC, apparent diffusion coefficient; MRS, magnetic resonance spectroscopy; SNR, signal-to-noise ratio; CT, computed tomography; FA, fractional anisotropy; CTH, capillary transit time heterogeneity.

* Corresponding author at: Department of Nuclear Medicine and Molecular Imaging, Medical Imaging Center, EB50, Postbus 30.001, University Medical Center Groningen, University of Groningen, Hanzeplein 1, 9700 RB Groningen, The Netherlands.

E-mail address: j.klos@umcg.nl (J. Kłos).

https://doi.org/10.1016/j.radonc.2019.05.020
0167-8140/

contributing to an even larger overall effect [9–12]. The resulting effects of radiotherapy-induced microvascular injury can be monitored by clinical examination as well as by magnetic resonance imaging (MRI). To detect radiotherapy-induced changes, MRI is generally considered as the most sensitive non-invasive technique with good clinical availability. Routine MRI techniques, such as T1-weighted imaging (T1), T2-weighted imaging (T2), fluid attenuated inversion recovery (FLAIR), diffusion-weighted imaging (DWI), dynamic contrast-enhanced (DCE), $T2^*$-weighted gradient echo ($T2^*$) and susceptibility-weighted imaging (SWI) can show oedema, cerebral microbleeds (CMBs), telangiectasias, cavernomas, white matter lesions (WML), lacunar infarcts, cortical atrophy and necrosis [13–19]. In the last decades, advanced imaging biomarkers reflecting microvascular integrity and function, such as quantitative susceptibility mapping (QSM), DSC-based (dynamic susceptibility contrast) vessel architectural imaging (VAI), arterial spin labelling (ASL), diffusion tensor imaging (DTI), intravoxel incoherent motion (IVIM) have emerged [20–25]. It seems straightforward to assume that both routine and emerging MRI techniques, alone or in combination, have the potential to provide sensitive imaging biomarkers which – directly or indirectly – reflect radiotherapy induced microvascular injury. However, to the best of our knowledge no recent systematic overview of available techniques and comparison concerning sensitivity and specificity of the individual techniques exist. The current work aims to provide such an overview and comparison, including a summary of the evidence regarding the relation with key clinical parameters and the optimal post-radiotherapy time window for each technique, in order to aid researchers in their choice of optimal (combinations of) MR techniques for their specific research aims.

Histopathophysiological processes underlying radiation-induced microvascular damage

Preclinical studies have shown that brain vessel endothelial hyperplasia and vessel wall thickening occur as early as 3 hours after irradiation with a dose of 100 Gy (gamma knife) [10]. Furthermore, a decrease in endothelial cell numbers was observed in rat brain after 5–200 Gy of local irradiation within the first 24 h and was not dependent on the applied dose [12]. Although the exact pathophysiological mechanism and timecourse of events has not been fully established, it is expected that in addition to endothelial damage, also a significant loss of oligodendrocytes occurs, which are the most radiation-damage prone glial cells [26]. Necrosis and apoptosis of oligodendrocytes result in myelin decrease around neurons, in turn resulting in impaired nerve conduction and reduced white matter integrity [26]. Astrocyte activation also changes upon irradiation, with astrocytes no longer being able to properly support neurons and the impulse transmission processes [26]. In addition, impaired and later hyalinized endothelium no longer properly delivers nutrients to glial and neuronal cells, which additionally exacerbates the dysfunction of those cells [26]. Finally, ischaemia and impaired microvascular oxygen extraction eventually can lead to radiation necrosis [26].

Radiotherapy-induced damage is classically divided into three timeframes [9,27,28], being acute, delayed and late-delayed injury. However, this classification is based primarily on clinical presentation and symptoms, and not on pathophysiological findings. Therefore, this classification is somewhat artificial with respect to the underlying pathophysiological processes. *Acute injury* presents from days to weeks following radiotherapy with headache, nausea, vomiting, fever, somnolence and more severe symptoms of brain herniation. Acute injury is believed to be caused especially by oedema and inflammation. The severity and commonness of this stage are usually less debilitating nowadays due to constant improvements in radiotherapy techniques. *Early-delayed injury* presents 1–6 months after radiotherapy and finds its roots in transient demyelination and neuroinflammation and clinically presents with mood fluctuations, cognitive deficits and somnolence in children, but also possibly in adults usually within the first 6 weeks following radiotherapy. Typically, symptoms related to this type of injury resolves within 1–3 months. Sometimes supplementary treatment with steroids is necessary. The most serious effect is *late-delayed injury* occurring >6 months after radiotherapy, which is often irreversible and caused by amassed vascular abnormalities, demyelination, loss of oligodendrocytes and neuronal precursors, gliosis, neuroinflammation and white matter necrosis, probably impelling each other [9,27,28]. Unfortunately, late-delayed changes so far cannot be reliably predicted based on the earlier clinical stages of brain injury [9,29]. Therefore, further research regarding the correlation of early events on the course and occurrence of late-delayed adverse effects is urgently required. Particularly imaging methods depicting the dynamics of microvascular changes over time after radiotherapy have the potential to bring us closer to a better understanding of radiotherapy-induced injury in general.

Quantification of radiotherapy-induced microvascular changes with routine MRI techniques

Oedema

Vasogenic brain oedema is an early radiotherapy side-effect resulting from an increased blood–brain barrier permeability [30]. Currently available advanced radiotherapy techniques applying limited and fractionated doses have decreased the risk of symptomatic and debilitating brain oedema, as well as the need for treatment [31]. The risk of developing oedema is higher with stereotactic radiosurgery (SRS) than with fractionated radiation therapy [32,33]. Because vasogenic brain oedema can be challenging to detect on MRI, its prevalence is not well known.

Conventional MRI often shows no oedema related changes but may demonstrate high T2/FLAIR signal and changes on diffusion weighted imaging [31]. With DCE-MRI the extravascular contrast leakage, representing oedema, was found to be the highest in the 6th week of radiotherapy and remained abnormal until 6 months after irradiation [34]. Additionally, early vascular injury visible on DCE-MRI seemed to predict late neurocognitive changes [34]. A similar correlation was found for changes within the hippocampal vasculature [35]. However, taking into consideration all the other possible factors able to cause and modulate oedema formation, such as chemotherapy, surgery and the presence of a necrotising or a recurring tumour, oedema itself is not a reliable indicator of radiotherapy-induced injury [13]. Therefore, the related problem of radiological differentiation of peritumoral oedema and necrosis from true tumour progression is being intensively investigated [36–39].

In conclusion, the uncertainties around the underlying cause of brain oedema on radiological images indicate that so far oedema cannot be considered a reliable follow-up marker of radiotherapy-induced microvascular complications.

Cerebral microbleeds

Cerebral microbleeds (CMBs) have important clinical implications. Associations have been found between the number of CMBs and increased risks of neurocognitive decline, stroke, intracranial haemorrhage and mortality [40]. Post-radiation CMBs seem to also affect neurocognition, including attention, executive functions, working memory and visual processing speed [41]. Notably,

a higher number of CMBs in temporal lobes leads to a higher risk for cognitive decline [42].

Histopathologically, CMBs most typically represent perivascular hemosiderin-filled macrophages resulting from a minor bleeding [43,44].

On MRI CMBs present as round or ovoid, nonlinear black lesions with blooming effect on T2*-weighted MRI and SWI [14]. They are most readily detectable on SWI which is highly sensitive to susceptibility changes of hemosiderin, to a lesser extent on T2*-weighted MRI, and are even harder to visualise on T2-weighted MRI [45] (Fig. 1). Lesions recognised as CMBs on MRI, histologically may represent other changes in up to 11–24% [46]. Lesions mimicking CMBs are small cavernomas, microaneurysms, microdissections, and microcalcifications [43,47–49]. Furthermore, using histology as the gold standard, up to half of the CMBs remain undetectable using 1.5–3T T2*-weighted MRI [43].

Radiotherapy-induced CMBs are common [7,41,50–52], but the prevalence depends on many factors including age of the study population, radiation doses and fields, types of MRI sequences and field strength used, and at which timepoint the follow-up took place. In a recent study deploying T2*-weighted and SWI sequences (1.5T or 3T), the prevalence was as high as 90% after a mean observational period of 13.5 years [52]. Using 7T MRI this number is much higher with CMBs being found in up to 100% of patients [53]. CMBs might be detected as soon as 3–4 months after radiotherapy onset, with a latency of up to 9 years (mean 33 months) [54], therefore representing both early-delayed and late-delayed injury. In the healthy general population the overall prevalence of CMBs increases with age; being 36% in the population >80 years, around 7% for 45–50 years and rare in children [55]. Although age at the time of receiving radiotherapy also seems to have an impact on the prevalence of CMBs, different studies provide conflicting information regarding the age dependency. This significantly complicates the use of CMBs as an imaging biomarker [41]. Furthermore, an apparent increase in the prevalence of CMBs is consistently seen in patients receiving higher radiation doses and/or volumes [41]. The prevalence of CMBs also increases each year following irradiation, expanding beyond the area of high-dose irradiation and crossing the hemisphere boundaries [50,56] (Fig. 2). Furthermore, since the changes emerge with different speed and amount in different patients with comparable radiotherapy treatment, individual predisposition probably also plays a role [57].

Currently, there are not enough data on possible differences between CMBs occurrence after photon vs proton therapy. Based on two available studies, the pattern of CMBs occurrence on MRI seems to be similar for photon and proton radiation therapy for both whole brain radiotherapy (WBRT) and focal radiation fields [50,58]. The first CMBs appeared already 3 months after proton therapy onset, with an increasing prevalence over time, especially within the first few years. Furthermore, the number of CMBs was related to risk factors, such as younger age and higher maximum radiation therapy dose [58]. In the case of proton therapy the highest amount of CMBs was found within the dose fields over 30 Gy [58].

In conclusion, regardless of certain limitations, so far CMBs seem to be the earliest radiological marker available on routine clinical imaging that both reflects microvascular radiotherapy-induced injury and correlates to delayed radiotherapy complications.

Telangiectasias

Telangiectasias as solitary findings were described in up to 20% of patients who underwent radiotherapy and were more common in a younger population [59]. The number of telangiectasia increased with time, and no evident dose-dependency was found [59]. However, clinical implications of radiation-induced telangiectasias remain unclear.

Telangiectasias are histologically dilated capillaries with thin endothelium interspersed with brain parenchyma [60]. They are free of calcifications, gliosis, external haemorrhage and hemosiderin-laden macrophages [60].

On T2*-weighted or SWI MRI telangiectasias demonstrate a hypointense signal due to the slow flow of blood rich in deoxyhaemoglobin [60,61], and can appear somewhat similar to CMBs. However, telangiectasias generally tend to be significantly bigger than CMBs and demonstrate homogeneous contrast enhancement [60,62].

In conclusion, the amount of studies and the number of patients participating in studies regarding the relation of telangiectasias with radiotherapy are not sufficient for a definite statement, but overall the evidence seems to support that telangiectasias are of minor relevance.

Cavernous malformations

Cavernous malformations resulting from radiotherapy are more at risk of symptomatic bleeding than cavernous malformations of other origins [15], resulting in a lifelong uncertainty for patients.

The risk of bleeding can be histopathologically explained by the presence of venous or capillary caverns lined with an endothelial

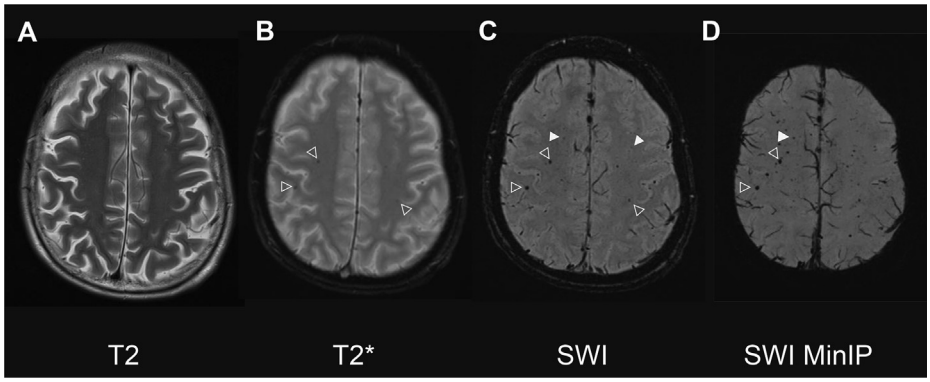

Fig. 1. Microbleeds on T2, T2*, SWI and SWI MinIP (Minimum intensity projection). A 24-year-old patient diagnosed with medulloblastoma in the posterior fossa. MRI obtained 19 years after initial resection followed by craniospinal irradiation and chemotherapy. The patient also received gamma knife radiosurgery 13 years after the first treatment. Multiple microbleeds have developed as a result of the treatment. The microbleeds are not visible on T2 (A). Some are shown on T2* (B; open arrowheads). The microbleeds are better detected on SWI, which demonstrates additional microbleeds not shown on T2* (C; closed arrowheads). The microbleeds are even better appreciated on MinIP SWI (D).

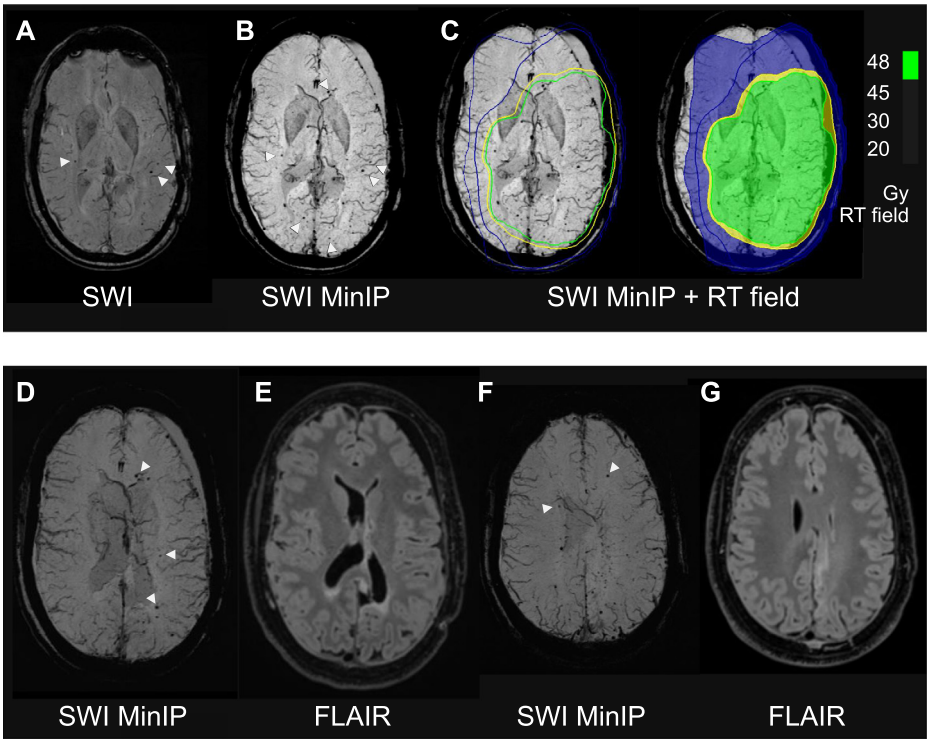

Fig. 2. Multiple microbleeds in relation to IMRT dose fields – also in areas with normal appearing FLAIR signal. A 47-year-old patient diagnosed with astrocytoma treated with surgery, radiotherapy and chemotherapy. Resection was performed on the left side at the age of 40, with MRI obtained 7 years after radiotherapy. Top row: Multiple microbleeds on SWI (A; arrowheads), better seen on MinIP reconstructions of the SWI (B; arrowheads). Asymmetry is observed in a number of microbleeds, left more than right and posterior more than anterior, which is explained by the radiotherapy dose distribution showing a close correlation with the microbleeds locations. Most microbleeds are visible within the 45 Gy isoline (C and D; yellow line). Bottom row: Multiple microbleeds are seen (D and F; arrowheads) in areas where the FLAIR signal is remarkably normal (E and G), although microbleeds were also present in areas with FLAIR abnormalities (e.g. periventricular left posterior; lowest arrowhead on A).

layer but lacking muscle and elastic components, which makes them fragile [63]. Additionally, cavernous malformations are not interspersed with normal brain parenchyma [63], in contrast with telangiectasias. Radiation-induced cavernous malformations are suggested to result from neoangiogenesis, following vessel occlusion, with wall hyalinisation, necrosis and concomitant mutations by some [15,64]. However, some researchers have suggested that cavernous malformations evolve from organising haematomas rather than proliferate directly from destructed vasculature [65]. Telangiectasias and cavernous malformations have been suspected to be different developmental stages with the same origin and risk of microbleeds [60,66].

On T2-weighted, T2*-weighted and SWI MRI the early stage cavernous malformations present as punctate hypointensities [67]. When more advanced, they demonstrate irregular intensity, popcorn-like enhancement and an incomplete hemosiderin rim [65] (Fig. 3).

The cumulative prevalence of cavernomas following brain irradiation after 10 years was found to be up to 43% [68]. The mean time from irradiation to the formation of typical multiple cavernomas varies from 3 to 12 years and cannot be considered homogenous [15,69]. Another study with T2*-weighted imaging also showed that higher radiation dose and a larger radiation field size led to a higher amount of cavernomas [70]. However, some

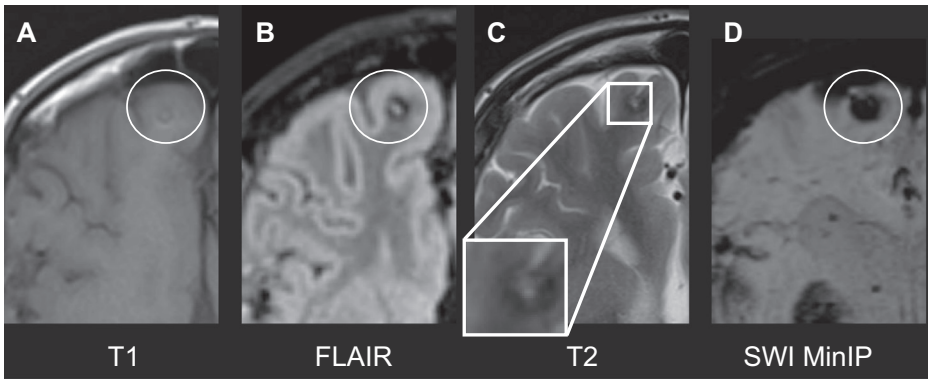

Fig. 3. Cavernous malformation after radiotherapy. The same patient as in Fig. 1. MRI obtained 19 years after radiotherapy, demonstrating a presumed small cavernous malformation. Subtle high T1 signal is shown centrally and peripherally (A). A hemosiderin rim is shown on FLAIR (B) and T2 (C). T2 also demonstrates the typical subtle popcorn/multicystic appearance. The lesion is most easily detected on SWI due to the contrast caused by iron in blood products (D). Enhancement (not shown) was absent. Although, histological confirmation is not available for the described lesion, it is worthy to note that the patient had previously undergone a resection of a different radiotherapy-induced cavernous malformation.

evidence exist that lower radiation doses lead to cell instability with a low level of apoptosis, resulting in a higher risk of cavernoma formation, while high-dose radiation results in intense cell apoptosis without a chance of cavernoma formation [69,71].

In conclusion, cavernous malformations visible on radiological imaging in their readily evolved form are considered a late-delayed complication and therefore are not useful as a timely predictive marker for future cognitive complications before the underlying processes become irreversible.

White matter lesions

Presence of white matter lesions (WML) and reduction in white matter volume clinically may lead to lower intelligence quotient (IQ) and deterioration of cognition [8,72–75]. The loss of white matter volume and deterioration of IQ, attention and academic performance increase with time passing from the radiotherapy onset [75]. Higher white matter volume loss is correlated with the radiation dose and younger age at the time of radiotherapy [75]. Neurocognitive decline after radiotherapy linked to white matter hyperintensities on T2-weighted MRI sequences, so-called radiation-induced leukoencephalopathy, is mostly represented by executive functions and episodic memory decline (subcortical frontal mode with information recovery deficiency), without correlation with the type of radiotherapy (focal or WBRT) [17]. In one study comparing children with ependymoma treated with proton beam radiation therapy (PBRT) or photon-based intensity-modulated radiation therapy (IMRT), more changes were observed in the proton beam group and in younger patients, which seems to be an effect of differences in relative biological effectiveness (RBE) [76,77]. Furthermore, in the study with pencil beam scanning proton therapy the prevalence of symptomatic WML in treated patients was as low as 3% [78].

Histopathological findings of WML are heterogeneous [79,80], despite a similar appearance on MRI, which indicates the complexity of the underlying processes, mutual dependency and dynamic influences between all the entities forming WML.

WML may represent degeneration and loss of myelin, axons, oligodendroglial cells and ependymal cells, as well as astrogliosis, activated macrophages, fibrohyalinotic vessel changes and cerebral ischemia with associated demyelination [79,80]. Those findings are all within the spectrum of WML, interpreted by some researchers as remains of ischemic microvascular processes, and in some cases resulting in accomplished lacunar infarcts [79].

Radiotherapy-induced WML are generally symmetrical in patients with total brain irradiation [81], similar to other neurological diseases evolving from microvascular impairment [82]. In other cases, the asymmetry of the WML reflects the asymmetry of the radiotherapy field in focal brain irradiation [83] (Fig. 4). Radiotherapy-induced WML typically spare the subcortical U-fibres [84,85] (Fig. 5), which may be helpful in distinguishing radiotherapy-induced white matter hyperintensities from tumour infiltrations, as both lead to T2-weighted and FLAIR-weighted hyperintensities. On conventional MRI sequences, WML become visible from a few months to several years after radiotherapy [30,86,87]. The prevalence of WML is unclear and differs significantly between studies [73,87,88]. However, novel localized radiotherapy techniques, such as SRS can reduce the risk for the occurrence of WML on MRI [89].

In conclusion, white matter lesions are an indirect marker of partial microvascular injury. They appear after radiotherapy with a highly varying delay and are mostly useful as additional radiological proof for readily apparent clinical symptoms.

Lacunar infarcts

Lacunar infarcts are commonly defined as fluid-filled cavities smaller than 15 mm in diameter of presumed vascular origin and therefore are considered one of the indicators for small vessel disease [90]. Capillary dysfunction may lead to impaired tissue oxygenation by diminished blood delivery, but also by means of a reduced oxygen extraction capacity over the capillary wall [91]. Although lacunar infarcts may be accompanied by clinical symptoms, in brain radiotherapy patients, lacunar infarcts were found to be predominantly silent without significant differences in observed IQ between groups with and without lacunar infarcts [92].

On MRI final lacunar infarcts present as small round or ovoid entities with cerebrospinal fluid (CSF) signal on all sequences and are surrounded by a thin rim of high T2 signal; this rim can only be appreciated on FLAIR images [93] (Fig. 6). In this context, they can look similar to wide perivascular spaces, especially at shared typical locations such as the level of the anterior commissure and basal ganglia, although perivascular spaces typically lack a rim of high signal intensity on FLAIR images [93]. Furthermore, newly appearing lesions favour a lacunar origin [90].

The incidence is higher for children younger than 5 years of age at the time of radiotherapy [92]. For the adult population, the incidence after receiving radiotherapy was found to be comparable to the incidence in the general population [16]. Lacunar infarcts seem to be late-delayed changes in most of the cases [92].

In conclusion, lacunar infarcts seem to only have a limited value in monitoring radiotherapy-induced microvascular damage, since they appear late, are infrequently present and are not correlated

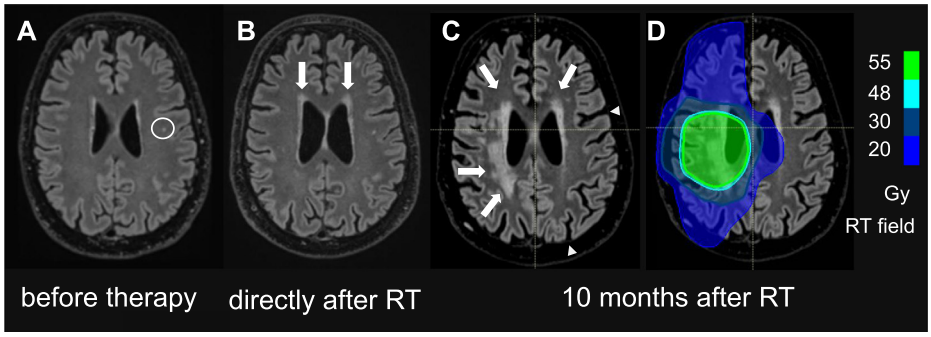

Fig. 4. White matter lesions with FLAIR abnormalities corresponding to radiotherapy field distribution. The same patient as Fig. 6 with a posterior tumour on the right side. MRI shows only minor white matter lesions before therapy (A; circle). A very subtle increase in periventricular FLAIR abnormalities can be observed directly following volumetric intensity modulated RT (VMAT). However, extensive microvascular damage with white matter changes is observed 10 months after radiotherapy. The changes are most pronounced in the area corresponding to the higher radiotherapy dose field (C; arrows). Sulci are also slightly more prominently depicted due to atrophy (C; see e.g. arrowheads). The white matter lesions correlate with the pre-treatment radiotherapy field, as most of the changes fall within the 55 Gy target volume (D; green) or the 30 Gy isoline (D; dark blue). The 20 Gy isoline is also marked (D; bright blue).

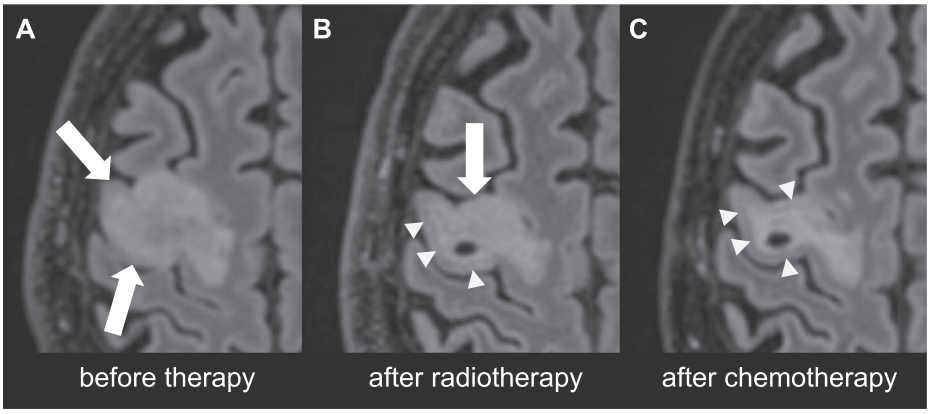

Fig. 5. Example of U-fiber involvement (tumour) and sparing (radiotherapy effect) on FLAIR MRI. A 69-year-old male with primary low-grade oligoastrocytoma IDH mutant and 1p/19q co-deleted. Tumour with mass effect and FLAIR abnormality is observed, also involving the subcortical U-fibers (A; arrow). After radiotherapy (B), mass effect is decreased and involvement of the subcortical U-fibers has disappeared posteriorly showing typical sparing of the subcortical U-fibers – demonstrated by hypointense normal signal between the cortex and FLAIR abnormalities (arrowhead). Involvement of the subcortical U-fibers persisted anteriorly (arrows) most likely due to residual tumour. The patient received additional chemotherapy, resulting in further decrease in mass-effect (C) and reduced involvement of the U-fibers anteriorly (arrowheads). Remaining FLAIR abnormalities are consistent with radiotherapy-induced microvascular damage, although follow-up is needed to exclude tumour recurrence.

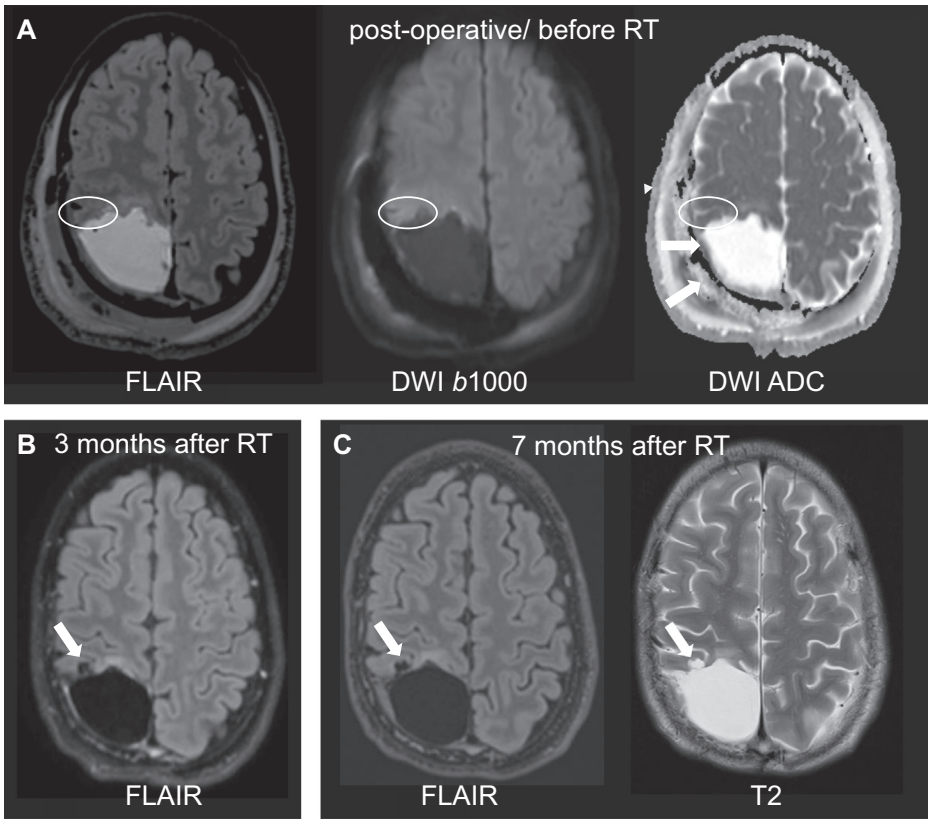

Fig. 6. Lacunar infarcts after radiotherapy. A 23-year-old patient diagnosed with anaplastic oligodendroglioma with 1p19q codeletion. First post-operative images showed no ischemia anterior-laterally of the resection cavity in the postcentral gyrus (A, circles). A lacunar infarct developed 3 months after radiotherapy (B, arrow). Follow-up at 7 months after radiotherapy showed further tissue loss with the typical imaging features of a lacunar infarct; a small cavity displaying CSF intensity as well as a rim of high signal on FLAIR and T2, with the rim best appreciated on FLAIR images (C, arrow).

with cognitive decline. However, the topic of lacunar infarcts probably requires further research, as the current literature on lacunar infarcts after brain irradiation can be considered fairly limited [94].

Radiation necrosis

Radiation necrosis is an extreme stage of radiation damage and is often a severe and irreversible process of cell death, involving both endothelium and white matter [19]. The reported prevalence of radiation necrosis varies between 3% and 64% [26]. Among novel radiotherapy techniques the occurrence of radiation necrosis is especially expected with SRS, due to delivery of high dose radiation with hypofractionation [95]. In the case of SRS up to half of the patients develop radiation necrosis, which is quite often symptomatic [95]. Although there have been only few studies considering radiation necrosis patterns following particle treatment in patients with brain tumours, there is a concern for higher rates of radiation necrosis after proton therapy because of a higher

relative RBE of protons [77,96,97]. However, a study using pencil beam scanning proton therapy revealed a relatively low incidence of symptomatic radiation necrosis (7%) [78]. Additionally, chemotherapy, especially when combining multiple chemotherapeutical agents, seems to be related to higher radiation necrosis rates in paediatric patients who underwent proton therapy [78,97]. Radiation necrosis may develop from weeks to even more than a decade after irradiation and can be life-threatening with mass effect, focal neurological symptoms and cognitive decline [98,99].

Histologically, radiation necrosis corresponds with haemorrhagic coagulative necrosis with vascular hyalinisation and reactive gliosis [98,100]. The clinical diagnosis of radiation necrosis is challenging regarding the lack of a clear definition, as it is currently described as the appearance of new neurological symptoms as well as radiological findings [100,101]. On conventional MRI radiation necrosis presents as a ring-enhancing lesion accompanied by oedema [102]. Since the radiological appearance of radiation necrosis is similar to that of tumour progression, these entities cannot be clearly distinguished on conventional MRI [102]. DWI derived ADC maps can be of help, but a more accurate differentiation has been shown using other MRI techniques like DSC imaging, DCE imaging, ASL and magnetic resonance spectroscopy (MRS), with MRS providing the highest sensitivity and specificity [102,103].

In conclusion, challenges related to distinguishing radiation necrosis from tumour progression, as well as the severity of brain tissue destruction in the area of radiation necrosis limits the value of radiation necrosis as a marker of radiotherapy-induced microvascular changes that are predictive of long-term complications.

Optimal cerebral microbleed detection with routine iron-specific MRI techniques

Because CMBs seem to be so far the most relevant clinically available potential early biomarker for radiotherapy-induced damage, having associations with delayed poorer cognitive function, we summarize below the rationale and approaches for optimal imaging of CMBs with conventional MRI.

T2*-weighted imaging and SWI are both susceptible to heme and non-heme iron, resulting in hypointensities on the SWI MRI image in area's with increased iron concentrations [104,105]. More specifically, the iron-susceptibility effect results from deoxyhaemoglobin, ferritin and hemosiderin, which are blood elements carrying exposed iron [57,104]. Oxygen in haemoglobin decreases the iron exposure and therefore the susceptibility effect; as a result arteries and arterioles are not as negatively contrasted on SWI as venous structures [57,104]. In line with this, increasing hemosiderin concentrations over time increases the sensitivity of SWI for CMBs detection, especially in the chronic phase of bleeding [106].

For detection of iron-positive lesions, SWI is preferred over T2*-weighted imaging, because of the higher overall sensitivity of SWI [45,67,107–109]. SWI can detect microbleeds of approximately the size of a typical voxel (1 mm^3) [106]. The superiority of SWI is based on combining both magnitude and phase information of the T2*-weighted gradient echo sequence [104]. SWI also provides a higher signal-to-noise ratio (SNR), and therefore can be acquired with higher spatial in-plane resolution and thinner sections compared to T2*-weighted imaging [108,110]. Also, SWI performed at 3T field strength still outperforms T2*-weighted imaging performed at a higher field strength of 7T [111]. In general, CMBs detection improves when using higher field strengths because of the increased sensitivity for detecting iron deposit induced susceptibility changes present in CMBs. This effect makes T2*-weighted and SWI at 3T and 7T MRI better tools for finding CMBs than similar sequences at 1.5T field strength [112,113]. However, the observed area with susceptibility changes overestimates the actual size of CMBs – the so-called blooming effect [111,112], which also scales with increasing field strength.

In one study no difference in detection of CMBs was found between 3T and 7T SWI MRI for the whole study group, but for some patients, 7T MRI showed more CMBs deeper in the brain [111]. SWI was also found to be more reliable and sensitive for detecting cavernous malformations, exposing twice the number of lesions compared to T2*-weighted imaging, and also far more sensitive than T2-weighted imaging, within multifocal and familial cases [67].

In general, the presence of a suspected CMB lesion detected with either T2*-weighted MRI or SWI correlates quite well with histopathological findings [44,45]. When it comes to CMBs being mimicked by calcifications, these ambiguities might be resolved using SWI-filtered phase images in combination with dual-energy CT scans [104,114]. SWI filtered-phase data distinguishes intensities of paramagnetic CMBs as hypointense and diamagnetic calcifications as hyperintense [104]. For excluding other deoxyhaemoglobin filled structures, QSM seems to be more sensitive.

Recent developments and future perspectives in MRI

Quantitative susceptibility mapping (QSM)

QSM is a post-processing technique that utilizes T2*-weighted gradient echo phase data to reconstruct a susceptibility map [20,21]. Iron deposits, calcifications and venous oxygen saturation can be assessed in a quantitative fashion with such a susceptibility map [20], which is not possible using SWI. This difference not only makes QSM more reliable than SWI when it comes to quantifying the iron concentration in a voxel, but also allows for a more accurate definition of the lesion location. Furthermore, QSM allows for a better estimation of the actual size of an observed lesion, a limitation seen with SWI and T2*-weighted MRI which overestimate lesion size because of the pronounced blooming effect in these sequences [20,115–117]. QSM seems to be the most reliable technique for iron quantification in longitudinal studies as well as in multicentre studies performed with different protocols, due to its higher intrinsic reproducibility [116].

QSM has the potential to better distinguish CMBs from veins, based on the stronger susceptibility effect resulting from different iron forms in a CMB [106]. In turn, this potentially allows for better differentiation between several histopathological entities of iron accumulation. Another benefit from QSM is allowing for differentiation between CMBs and calcifications, which is not always possible with SWI due to aliasing [21]. Applying iron oxide nanoparticles based contrast agents together with quantitative T1, T2 and T2* relaxation time measurements and QSM, even seems to enable the assessment of cerebral blood volume, mean vessel size and microvascular angiogenesis [116,118–121]. However, the downsides of QSM are lengthy imaging postprocessing times and the need for manual detection and evaluation of all visible lesions, making it time-consuming and potentially vulnerable for interobserver variability [122]. Those issues are probably going to be solved by automatic quantification in the future [122]. Currently QSM images can also be influenced by the artefacts from the regions neighbouring the skull [122], similarly to SWI.

QSM has already been shown to be superior to SWI concerning detection of CMBs and diffuse axonal injury in traumatic brain injury patients [106], as well as superior in revealing CMBs from underlying unstable aneurysms [122,123] and cerebral cavernous malformations [124–126]. Those findings underscore the potential

benefit of QSM for the detection of radiotherapy-induced microvascular complications, leading to an earlier and more exact assessment of risk for delayed complications in brain tumour patients.

In summary the major potential advantages of QSM are the ability to quantitatively assess CMBs over time and its robustness due to insensitivity to technical differences between different scanners [127]. However, to what extent these advantages hold true in clinical use should be further validated before routine clinical implementation can be considered.

Diffusion tensor imaging (DTI)

DTI derived fractional anisotropy (FA) is so far the best imaging biomarker for tracking early white matter disruptions [128], which as mentioned before, seem to indirectly reflect microvascular pathology. Although DTI shows no significant differences between regions with different radiation dose within the first month following radiochemotherapy treatment, the images become abnormal after 4–6 months [24]. Interestingly, FA was also reduced in the normal-appearing areas on T2-weighted MRI [128], as early as 3 months after irradiation and partially returned to normal within 14 months from irradiation in adults treated with adjuvant radiotherapy only [86]. Furthermore, it has been suggested that DTI changes also correlate with neurocognitive deterioration [128–134]. Dose-dependence and prevalence of white matter changes as assessed by DTI differ between studies, but they seem to occur even after low doses of radiotherapy (5–10 Gy) [24,135,136]. White matter disruptions seem to be mainly due to progressive dose-dependent demyelination, and within the first months occur mainly in high dose areas [136]. After 32 weeks from radiotherapy onset, the process becomes diffuse and is also concomitant with mild axonal fibre injury [136]. Another DTI based study found remarkable extracellular changes, suggesting that changed vascular permeability and neuroinflammation are both contributors to the white matter disruption [24]. A recent study employing DTI and resting state functional MRI demonstrated the existence of a dynamic multifocal process of overlapping vasculopathy and demyelination, in which vasculopathy dominates the early stages, followed by demyelination [137], in turn suggesting that the above described heterogeneous changes may resolve or progress, depending on the processes of neuroprotection and compensation.

That also implies that it will be essential to simultaneously assess both microvascular changes using MR microvascular perfusion techniques as well as white matter changes with diffusion sensitive MRI approaches in the context of radiotherapy monitoring, because of observed delays in the onset of demyelination after radiotherapy induced microvascular changes [137].

Novel dynamic susceptibility-weighted contrast-enhanced imaging techniques

Single (gradient) echo dynamic susceptibility-weighted (DSC)-based acquisitions can be post-processed to generate a novel imaging biomarker reflecting microvascular flow heterogeneity, called capillary transit time heterogeneity (CTH) [138]. In a wide variety of pathological conditions CTH has been shown to increase significantly and with greater general sensitivity than other functional MR-derived imaging biomarkers [91,139–141]. Use of CTH in radiotherapy planning and response evaluation has been highly limited, but it holds great promise due to its expected sensitivity to early changes.

Dual echo (spin-echo/gradient-echo) variants of the DSC technique can be used to derive a similar, yet slightly different, imaging biomarker, reflecting more microvascular architectural changes than capillary flow heterogeneity alone, using the ratio of gradient echo versus spin echo relaxation rates over time [22]. This recently developed technique called vessel architectural imaging (VAI) enables the visualisation of susceptibility effects induced by microvessels even <10 μm radius, including capillaries [22]. VAI was primarily used for assessing glioblastoma vessels' response to anti-angiogenic therapy by evaluating changes in tissue microvascular architecture and oxygenation in the tumour before and after treatment. Observed stabilisation of microvascular architecture and oxygen levels after treatment, meaning a decrease in microvessel leakage and hypoxia, local shunting or closed microvessels, indicates that this method can outperform all other commonly used MR sequences regarding prediction of overall survival [142]. Similar techniques based on spin-echo and gradient-echo imaging of vessel size, oxygen metabolism and neovascularisation, were also found useful in glioma grading [143,144]. Due to its high sensitivity to change, VAI could potentially be used to assess early post-radiation dynamic changes in brain microvasculature before later changes emerge.

Arterial spin labelling (ASL)

ASL is a non-invasive flow imaging technique without the need for intravenous contrast medium administration, with the potential for estimating cerebral perfusion changes in capillaries after radiotherapy [145]. A study with ASL after focal brain radiation showed an early decrease in grey matter cerebral blood flow in primary brain tumour patients, more prominent in the areas receiving a higher radiation dose [146]. It is believed to be caused by early endothelial cell number depletion, in turn leading to capillary wall instability and occlusion [34,146,147]. ASL was also found to be useful for the differentiation between low and high-grade gliomas [148,149]. ASL-based brain tumour vascular density estimation seems to correlate with corresponding histopathological findings [150]. However, to the best of our knowledge, currently no clear evidence exists that ASL can provide detailed microvascular information beyond mean density, such as microvascular architecture which can be provided by DSC-MRI.

Intravoxel incoherent motion (IVIM)

IVIM quantifies microvascular perfusion information based on local voxel readouts, independent on arterial input function [25,151,152]. This method was found to be sensitive for perfusion changes of vasoconstriction and vasodilatation due to blood oxygenation level changes [25]. In comparison with DSC, IVIM possibly presents images with a higher resolution not being dependent on the contrast leakage as no i.v. contrast administration is needed for IVIM [152]. The difference should be especially prominent within areas with pathological changes and impaired blood–brain barrier [152]. IVIM seems to be based on chaotic blood flow in small vessels and capillaries, without signal contamination from large vessels as is the case in DSC [25,152].

IVIM has been applied with promising results for perfusion imaging in several organs and diseases [152], as well as in glioma grading [153] and tumour progression [37], as an addition to other techniques. However, it is not as attractive for the brain due to small cerebral perfusion fraction (5%) [154] and resulting low signal-to-noise ratio [25]. However, a study on cerebral small vessel disease aiming to assess the brain microvasculature and parenchymal microstructure with IVIM unexpectedly revealed increased perfusion volume fraction in relation to disease severity [155]. The latest study combining ASL and IVIM imaging has brought more insight into the complexity of IVIM measurements [154], showing the advantages of combining different methods.

Future directions

Novel promising MRI techniques available for research are yet to be implemented for the purpose of (early) detection of radiotherapy complications. Studies using DTI not only have changed our perception of the timecourse of white matter integrity disturbances, with great advantages over traditional FLAIR and T2-weighted imaging for WML, but also gave more insight into the relation of WML to cognitive changes. The cerebral changes detected with conventional MRI all seem to be a result of a complex process, in which endothelium plays a key role. Radiologically detectable dynamics of microvascular changes under the influence of brain radiotherapy is still a missing piece of the puzzle, and this part is yet to be properly investigated. Following microvascular changes during radiotherapy treatment over time could not only improve decision-making regarding further radiation treatment planning (adaptive radiotherapy) but could also facilitate research on drugs reversing the early pathological process. Furthermore, comparing early microvascular damage in patients treated with photon and proton therapy could accelerate the understanding of why proton therapy treatment for low-grade gliomas in adults may be advantageous regarding cognitive changes within the 5 year follow-up period after radiotherapy [156].

The outlined research should preferably be performed in low-grade brain tumour patient populations, for obtaining a better assessment of the correlations between early microvascular changes and delayed cognitive outcomes, as this group of mostly young adult patients is generally neurologically and neurocognitively intact at the time of diagnosis and has a relatively high survival and long lifespan.

Another highly interesting approach is to combine different MRI techniques and derived imaging biomarkers within the same patient, as this can lead to a better understanding of all facets of the radiation damage. Combining advanced perfusion techniques with DTI, QSM or IVIM have the potential to provide quantitative results that better reflect the multifactorial nature of the underlying processes.

Conclusions

The body of knowledge regarding the consequences of brain radiotherapy is expanding, as well as the range of emerging novel MRI techniques with a high potential to provide novel insights. However, using MR-derived imaging biomarkers for prediction and prevention of early and long-term radiotherapy side effects, such as microvascular-injury-related changes, remain highly challenging. Because of the advent of new oncological therapies, the overall survival of patients with brain tumours continues to increase, making early detection and prediction of side-effects also increasingly relevant and urgent. MRI techniques routinely available to clinicians often lack sensitivity and specificity for the detection of early changes, making the choice of the correct technique for specific research questions ever more important. The current situation poses a need for early MRI biomarkers to predict long-term outcome after radiotherapy. That would allow early prevention of cognitive problems and could open the door for MRI-guided adaptive radiotherapy, using an optimized approach to minimise long-term effects of radiotherapy on healthy brain tissue and simultaneously pave the way for validation of potentially protective pharmaceutical interventions.

Finally, we conclude that a single current or future MRI technique will probably not be able to provide all answers needed, whereas integration of multi-technique/sequence derived imaging biomarkers could provide a workable path forward, overcoming several of the current limitations of individual biomarkers for the assessment of radiotherapy-induced microvascular injury.

Funding

None.

Declaration of Competing Interest

The authors declare that there is no conflict of interest.

Acknowledgements

None.

References

[1] Gondi V, Yock TI, Mehta MP. Proton therapy for paediatric CNS tumours-improving treatment-related outcomes. Nat Rev Neurol 2016;12:334–45. https://doi.org/10.1038/nrneurol.2016.70.
[2] Buckner JC, Shaw EG, Pugh SL, Chakravarti A, Gilbert MR, Barger GR, et al. Radiation plus procarbazine, CCNU, and vincristine in low-grade glioma. N Engl J Med 2016;374:1344–55. https://doi.org/10.1056/NEJMoa1500925.
[3] Youland RS, Kreofsky CR, Schomas DA, Brown PD, Buckner JC, Laack NN. The impact of adjuvant therapy for patients with high-risk diffuse WHO grade II glioma. J Neurooncol 2017;135:535–43. https://doi.org/10.1007/s11060-017-2599-1.
[4] Reifenberger G, Wirsching HG, Knobbe-Thomsen CB, Weller M. Advances in the molecular genetics of gliomas-implications for classification and therapy. Nat Rev Clin Oncol 2017;14:434–52. https://doi.org/10.1038/nrclinonc.2016.204.
[5] Buckner J, Giannini C, Eckel-Passow J, Lachance D, Parney I, Laack N, et al. Management of diffuse low-grade gliomas in adults – use of molecular diagnostics. Nat Rev Neurol 2017;13:340–51. https://doi.org/10.1038/nrneurol.2017.54.
[6] Claus EB, Walsh KM, Wiencke JK, Molinaro AM, Wiemels JL, Schildkraut JM, et al. Survival and low-grade glioma: the emergence of genetic information. Neurosurg Focus 2015;38:E6. https://doi.org/10.3171/2014.10.FOCUS12367.
[7] Belliveau JG, Bauman GS, Tay KY, Ho D, Menon RS. Initial investigation into microbleeds and white matter signal changes following radiotherapy for low-grade and benign brain tumors using ultra-high-field mri techniques. Am J Neuroradiol 2017;38:2251–6. https://doi.org/10.3174/ajnr.A5395.
[8] Ajithkumar T, Price S, Horan G, Burke A, Jefferies S. Prevention of radiotherapy-induced neurocognitive dysfunction in survivors of paediatric brain tumours: the potential role of modern imaging and radiotherapy techniques. Lancet Oncol 2017;18:e91–e100. https://doi.org/10.1016/S1470-2045(17)30030-X.
[9] Makale MT, McDonald CR, Hattangadi-Gluth JA, Kesari S. Mechanisms of radiotherapy-associated cognitive disability in patients with brain tumours. Nat Rev Neurol 2016;13:52–64. https://doi.org/10.1038/nrneurol.2016.185.
[10] Yang T, Wu SL, Liang JC, Rao ZR, Ju G. Time-dependent astroglial changes after gamma knife radiosurgery in the rat forebrain. Neurosurgery 2000;47:407–16.
[11] Li Y-Q, Chen P, Haimovitz-Friedman A, Reilly RM, Wong CS. Endothelial apoptosis initiates acute blood-brain barrier disruption after ionizing radiation. Cancer Res 2003;63:5950–6.
[12] Ljubimova NV, Levitman MK, Plotnikova ED, Eidus LK. Endothelial cell population dynamics in rat brain after local irradiation. Br J Radiol 1991;64:934–40. https://doi.org/10.1259/0007-1285-64-766-934.
[13] Hein PA, Eskey CJ, Dunn JF, Hug EB. Diffusion-weighted imaging in the follow-up of treated high-grade gliomas: tumor recurrence versus radiation injury. Am J Neuroradiol 2004;25:201–9. https://doi.org/10.1063/1.1679672.
[14] Greenberg SM, Vernooij MW, Cordonnier C, Viswanathan A, Al-Shahi Salman R, Warach S, et al. Cerebral microbleeds: a guide to detection and interpretation. Lancet Neurol 2009;8:165–74. https://doi.org/10.1016/S1474-4422(09)70013-4.
[15] Cutsforth-Gregory JK, Lanzino G, Link MJ, Brown Jr RD, Flemming KD. Characterization of radiation-induced cavernous malformations and comparison with a nonradiation cavernous malformation cohort. J Neurosurg 2015;122:1214–22. https://doi.org/10.3171/2015.1.JNS141452. Disclosure.
[16] Molad JA, Blumenthal DT, Bokstein F, Findler M, Finkel I, Bornstein NM, et al. Mechanisms of post-radiation injury: cerebral microinfarction not a significant factor. J Neurooncol 2017;131:277–81. https://doi.org/10.1007/s11060-016-2291-x.
[17] Bompaire F, Lahutte M, Buffat S, Soussain C, Ardisson AE, Terziev R, et al. New insights in radiation-induced leukoencephalopathy: a prospective cross-sectional study. Support Care Cancer 2018;26:4217–26. https://doi.org/10.1007/s00520-018-4296-9.
[18] Seibert TM, Karunamuni R, Kaifi S, Burkeen J, Connor M, Krishnan AP, et al. Cerebral Cortex Regions Selectively Vulnerable to Radiation Dose-Dependent

Atrophy. Int J Radiat Oncol Biol Phys 2017;97:910–8. https://doi.org/10.1016/j.ijrobp.2017.01.005.
[19] Wang S, Tryggestad E, Zhou T, Armour M, Wen Z, Fu DX, et al. Assessment of MRI parameters as imaging biomarkers for radiation necrosis in the rat brain. Int J Radiat Oncol Biol Phys 2012;83:e431–6. https://doi.org/10.1016/j.ijrobp.2011.12.087.
[20] Haacke EM, Liu S, Buch S, Zheng W, Wu D, Ye Y. Quantitative susceptibility mapping: current status and future directions. Magn Reson Imaging 2015;33:1–25. https://doi.org/10.1016/j.mri.2014.09.004.
[21] Schweser F, Deistung A, Lehr BW, Reichenbach JR. Differentiation between diamagnetic and paramagnetic cerebral lesions based on magnetic susceptibility mapping. Med Phys 2010;37:5165–78. https://doi.org/10.1118/1.3481505.
[22] Emblem KE, Mouridsen K, Bjornerud A, Farrar CT, Jennings D, Borra RJH, et al. Vessel architectural imaging identifies cancer patient responders to anti-angiogenic therapy. Nat Med 2013;19:1178–83. https://doi.org/10.1038/nm.3289.
[23] Wang YL, Chen S, Xiao HF, Li Y, Wang Y, Liu G, et al. Differentiation between radiation-induced brain injury and glioma recurrence using 3D pCASL and dynamic susceptibility contrast-enhanced perfusion-weighted imaging. Radiother Oncol 2018;129:68–74. https://doi.org/10.1016/j.radonc.2018.01.009.
[24] Connor M, Karunamuni R, McDonald C, White N, Pettersson N, Moiseenko V, et al. Dose-dependent white matter damage after brain radiotherapy. Radiother Oncol 2016;121:209–16. https://doi.org/10.1016/j.radonc.2016.10.003.
[25] Federau C, Maeder P, O'Brien K, Browaeys P, Meuli R, Hagmann P. Quantitative measurement of brain perfusion with intravoxel incoherent motion MR imaging. Radiology 2012;265:874–81. https://doi.org/10.1148/radiol.12120584.
[26] Furuse M, Nonoguchi N, Kawabata S, Miyatake SI, Kuroiwa T. Delayed brain radiation necrosis: pathological review and new molecular targets for treatment. Med Mol Morphol 2015;48:183–90. https://doi.org/10.1007/s00795-015-0123-2.
[27] Sheline GE, Wara WM, Smith V. Therapeutic irradiation and brain injury. Int J Radiat Oncol Biol Phys 1980;6:1215–28.
[28] Tofilon PJ, Fike JR. The radioresponse of the central nervous system: a dynamic process. Radiat Res 2000;153:357–70.
[29] Robbins ME, Brunso-Bechtold JK, Peiffer AM, Tsien CI, Bailey JE, Marks LB. Imaging radiation-induced normal tissue injury. Radiat Res 2012;177:449–66. https://doi.org/10.1667/RR2530.1.
[30] Walker AJ, Ruzevick J, Malayeri AA, Rigamonti D, Lim M, Redmond KJ, et al. Postradiation imaging changes in the CNS: how can we differentiate between treatment effect and disease progression? Futur Oncol 2014;10:1277–97. https://doi.org/10.2217/fon.13.271.
[31] Brandsma D, Stalpers L, Taal W, Sminia P, van den Bent MJ. Clinical features, mechanisms, and management of pseudoprogression in malignant gliomas. Lancet Oncol 2008;9:453–61. https://doi.org/10.1016/S1470-2045(08)70125-6.
[32] Morgan TM, Zaenger D, Switchenko JM, Eaton BR, Crocker IR, Ali AN, et al. Fractionated radiotherapy is associated with lower rates of treatment-related edema than stereotactic radiosurgery in magnetic resonance imaging–defined meningiomas. World Neurosurg 2019;121:e640–6. https://doi.org/10.1016/j.wneu.2018.09.179.
[33] Harat M, Lebioda A, Lasota J, Makarewicz R. Evaluation of brain edema formation defined by MRI after LINAC-based stereotactic radiosurgery. Radiol Oncol 2017;51:137–41. https://doi.org/10.1515/raon-2017-0018.
[34] Cao Y, Tsien CI, Sundgren PC, Nagesh V, Normolle D, Buchtel H, et al. Dynamic contrast-enhanced magnetic resonance imaging as a biomarker for prediction of radiation-induced neurocognitive dysfunction. Clin Cancer Res 2009;15:1747–54. https://doi.org/10.1158/1078-0432.CCR-08-1420.
[35] Farjam R, Pramanik P, Aryal MP, Srinivasan A, Chapman CH, Tsien CI, et al. A radiation-induced hippocampal vascular injury surrogate marker predicts late neurocognitive dysfunction. Int J Radiat Oncol Biol Phys 2015;93:908–15. https://doi.org/10.1016/j.ijrobp.2015.08.014.
[36] Hansen MR, Pan E, Wilson A, McCreary M, Wang Y, Stanley T, et al. Post-gadolinium 3-dimensional spatial, surface, and structural characteristics of glioblastomas differentiate pseudoprogression from true tumor progression. J Neurooncol 2018;139:731–8. https://doi.org/10.1007/s11060-018-2920-7.
[37] Liu ZC, Yan LF, Hu YC, Sun YZ, Tian Q, Nan HY, et al. Combination of IVIM-DWI and 3D-ASL for differentiating true progression from pseudoprogression of Glioblastoma multiforme after concurrent chemoradiotherapy: Study protocol of a prospective diagnostic trial. BMC Med Imaging 2017;17:1–7. https://doi.org/10.1186/s12880-017-0183-y.
[38] Thust SC, van den Bent MJ, Smits M. Pseudoprogression of brain tumors. J Magn Reson Imaging 2018;48:571–89. https://doi.org/10.1002/jmri.26171.
[39] Tsang DS, Murphy ES, Lucas JT, Lagiou P, Acharya S, Merchant TE. Pseudoprogression in pediatric low-grade glioma after irradiation. J Neurooncol 2017;135:371–9. https://doi.org/10.1007/s11060-017-2583-9.
[40] Charidimou A, Shams S, Romero JR, Ding J, Veltkamp R, Horstmann S, et al. Clinical significance of cerebral microbleeds on MRI: a comprehensive meta-analysis of risk of intracerebral hemorrhage, ischemic stroke, mortality, and dementia in cohort studies (v1). Int J Stroke 2018;13:454–68. https://doi.org/10.1177/1747493017751931.
[41] Roddy E, Sear K, Felton E, Tamrazi B, Gauvain K, Torkildson J, et al. Presence of cerebral microbleeds is associated with worse executive function in pediatric brain tumor survivors. Neuro Oncol 2016;18:1548–58. https://doi.org/10.1093/neuonc/now163.
[42] Shen Q, Lin F, Rong X, Yang W, Li Y, Cai Z, et al. Temporal cerebral microbleeds are associated with radiation necrosis and cognitive dysfunction in patients treated for nasopharyngeal carcinoma. Int J Radiat Oncol Biol Phys 2016;94:1113–20. https://doi.org/10.1016/j.ijrobp.2015.11.037.
[43] Haller S, Montandon ML, Lazeyras F, Scheffler M, Meckel S, Herrmann FR, et al. Radiologic-histopathologic correlation of CEREBRAL microbleeds using pre-mortem and post-mortem MRI. PLoS One 2016;11:1–11. https://doi.org/10.1371/journal.pone.0167743.
[44] Fazekas F, Kleinert R, Roob G, Kleinert G, Kapeller P, Schmidt R, et al. Histopathologic analysis of foci of signal loss on gradient-echo T2*-weighted MR images in patients with spontaneous intracerebral hemorrhage: Evidence of microangiopathy-related microbleeds. Am J Neuroradiol 1999;20:637–42. https://doi.org/10.1016/S1471-4906(01)02051-8.
[45] Shams S, Martola J, Cavallin L, Granberg T, Shams M, Aspelin P, et al. SWI or T2*: which MRI sequence to use in the detection of cerebral microbleeds? The Karolinska Imaging Dementia Study. Am J Neuroradiol 2015;36:1089–95. https://doi.org/10.3174/ajnr.A4248.
[46] Haller S, Vernooij MW, Kuijer JPA, Larsson E-M, Jäger HR, Barkhof F. Cerebral microbleeds: Imaging and Clinical Significance. Radiology 2018;287:11–28. https://doi.org/10.1148/radiol.2018170803.
[47] Shoamanesh A, Kwok CS, Benavente O. Cerebral microbleeds: histopathological correlation of neuroimaging. Cerebrovasc Dis 2011;32:528–34. https://doi.org/10.1159/000331466.
[48] Tatsumi S, Shinohara M, Yamamoto T. Direct comparison of histology of microbleeds with postmortem MR images: a case report. Cerebrovasc Dis 2008;26:142–6. https://doi.org/10.1159/000139661.
[49] Schrag M, McAuley G, Pomakian J, Jiffry A, Tung S, Mueller C, et al. Correlation of hypointensities in susceptibility-weighted images to tissue histology in dementia patients with cerebral amyloid angiopathy: a postmortem MRI study. Acta Neuropathol 2010;119:291–302. https://doi.org/10.1007/s00401-009-0615-z.
[50] Roongpiboonsopit D, Kuijf HJ, Charidimou A, Xiong L, Vashkevich A, Martinez-Ramirez S, et al. Evolution of cerebral microbleeds after cranial irradiation in medulloblastoma patients. Neurology 2017;88:789–96. https://doi.org/10.1212/WNL.0000000000003631.
[51] Passos J, Nzwalo H, Valente M, Marques J, Azevedo A, Netto E, et al. Microbleeds and cavernomas after radiotherapy for paediatric primary brain tumours. J Neurol Sci 2017;372:413–6. https://doi.org/10.1016/j.jns.2016.11.005.
[52] Neu MA, Tanyildizi Y, Wingerter A, Henninger N, El Malki K, Alt F, et al. Susceptibility-weighted magnetic resonance imaging of cerebrovascular sequelae after radiotherapy for pediatric brain tumors. Radiother Oncol 2018;127:280–6. https://doi.org/10.1016/j.radonc.2018.03.010.
[53] Morrison MA, Hess CP, Clarke JL, Butowski N, Chang SM, Molinaro AM, et al. Risk factors of radiotherapy-induced cerebral microbleeds and serial analysis of their size compared with white matter changes: a 7T MRI study in 113 adult patients with brain tumors. J Magn Reson Imaging 2019:1–10. https://doi.org/10.1002/jmri.26651.
[54] Tanino T, Kanasaki Y, Tahara T, Michimoto K, Kodani K, Kakite S, et al. Radiation-induced microbleeds after cranial irradiation: evaluation by phase-sensitive magnetic resonance imaging with 3.0 Tesla. Yonago. Acta Med 2013;56:7–12.
[55] Poels MMF, Vernooij MW, Ikram MA, Hofman A, Krestin GP, Van Der Lugt A, et al. Prevalence and risk factors of cerebral microbleeds: sn update of the rotterdam scan study. Stroke 2010:41. https://doi.org/10.1161/STROKEAHA.110.595181.
[56] Lupo JM, Chuang CF, Chang SM, Barani IJ, Jimenez B, Hess CP, et al. Susceptibility-weighted imaging to assess the effects of radiotherapy on normal-appearing brain in patients with glioma. Int J Radiat Oncol Biol Phys 2012;82.. https://doi.org/10.1016/j.ijrobp.2011.05.046.
[57] Peters S, Pahl R, Claviez A, Jansen O. Detection of irreversible changes in susceptibility-weighted images after whole-brain irradiation of children. Neuroradiology 2013;55:853–9. https://doi.org/10.1007/s00234-013-1185-2.
[58] Kralik SF, Mereniuk TR, Grignon L, Shih CS, Ho CY, Finke W, et al. Radiation-induced cerebral microbleeds in pediatric patients with brain tumors treated with proton radiation therapy. Int J Radiat Oncol Biol Phys 2018;102:1465–71. https://doi.org/10.1016/j.ijrobp.2018.07.2016.
[59] Koike S, Aida N, Hata M, Fujita K, Ozawa Y, Inoue T. Asymptomatic radiation-induced telangiectasia in children after cranial irradiation: frequency, latency, and dose relation. Radiology 2004;230:93–9. https://doi.org/10.1148/radiol.2301021143.
[60] Castillo M, Morrison T, Shaw JA, Bouldin TW. MR imaging and histologic features of capillary telangiectasia of the basal ganglia. Am J Neuroradiol 2001;22:1553–5.
[61] Yoshida Y, Terae S, Kudo K, Tha KK, Imamura M, Miyasaka K. Capillary telangiectasia of the brain stem diagnosed by susceptibility-weighted imaging. J Comput Assist Tomogr 2006;30:980–2. https://doi.org/10.1097/01.rct.0000220810.81221.27.
[62] Lee RR, Becher MW, Benson ML, Rigamonti D. Brain capillary telangiectasia: MR imaging appearance and clinicohistopathologic findings. Radiology 1997;205:797–805. https://doi.org/10.1148/radiology.205.3.9393538.
[63] Jehi LE, Palmini A, Aryal U, Coras R, Paglioli E. Cerebral cavernous malformations in the setting of focal epilepsies: Pathological findings,

clinical characteristics, and surgical treatment principles. Acta Neuropathol 2014;128:55–65. https://doi.org/10.1007/s00401-014-1294-y.
[64] Larson JJ, Ball WS, Bove KE, Crone KR, Tew JM. Formation of intracerebral cavernous malformations after brain radiation treatment for central nervous system neoplasia in children. J Neurosurg 1998;88:51–6. https://doi.org/10.3171/jns.1998.88.1.0051.
[65] Cha YJ, Nahm JH, Ko JE, Shin HJ, Chang JH, Cho NH, et al. Pathological evaluation of radiation-induced vascular lesions of the brain: distinct from de novo cavernous hemangioma. Yonsei Med J 2015;56:1714–20. https://doi.org/10.3349/ymj.2015.56.6.1714.
[66] Rigamonti D, Johnson PC, Spetzler RF, Hadley MN, Drayer BP. Cavernous malformations and capillary telangiectasia: a spectrum within a single pathological entity. Neurosurgery 1991;28:60–4. https://doi.org/10.1227/00006123-199101000-00010.
[67] De Champfleur NM, Langlois C, Ankenbrandt WJ, Le Bars E, Leroy MA, Duffau H, et al. Magnetic resonance imaging evaluation of cerebral cavernous malformations with susceptibility-weighted imaging. Neurosurgery 2011;68:641–7. https://doi.org/10.1227/NEU.0b013e31820773cf.
[68] Lew SM, Morgan JN, Psaty E, Lefton DR, Allen JC, Abbott R. Cumulative incidence of radiation-induced cavernomas in long-term survivors of medulloblastoma. J Neurosurg Pediatr 2006;104:103–7. https://doi.org/10.3171/ped.2006.104.2.103.
[69] Di Giannatale A, Morana G, Rossi A, Cama A, Bertoluzzo L, Barra S, et al. Natural history of cavernous malformations in children with brain tumors treated with radiotherapy and chemotherapy. J Neurooncol 2014;117:311–20. https://doi.org/10.1007/s11060-014-1390-9.
[70] Li L, Mugikura S, Kumabe T, Murata T, Mori E, Takase K, et al. A comparative study of the extent of cerebral microvascular injury following whole-brain irradiation versus reduced-field irradiation in long-term survivors of intracranial germ cell tumors. Radiother Oncol 2015;117:302–7. https://doi.org/10.1016/j.radonc.2015.09.017.
[71] Keezer M, Del Maestro R. Radiation-induced cavernous hemangiomas: case report and literature review. Can J Neurol Sci 2009;36:303–10. https://doi.org/10.1017/S0317167100007022.
[72] Padovani L, André N, Constine LS, Muracciole X. Neurocognitive function after radiotherapy for paediatric brain tumours. Nat Rev Neurol 2012;8:578–88. https://doi.org/10.1038/nrneurol.2012.182.
[73] Fouladi M, Chintagumpala M, Laningham FH, Ashley D, Kellie SJ, Langston JW, et al. White matter lesions detected by magnetic resonance imaging after radiotherapy and high-dose chemotherapy in children with medulloblastoma or primitive neuroectodermal tumor. J Clin Oncol 2004;22:4551–60. https://doi.org/10.1200/JCO.2004.03.058.
[74] Mulhern RK, Palmer SL, Reddick WE, Glass JO, Kun LE, Taylor J, et al. Risks of young age for selected neurocognitive deficits in medulloblastoma are associated with white matter loss. J Clin Oncol 2001;19:472–9. https://doi.org/10.1200/JCO.2001.19.2.472.
[75] Reddick WE, Taghipour DJ, Glass JO, Ashford J, Xiong X, Wu S, et al. Prognostic factors that increase the risk for reduced white matter volumes and deficits in attention and learning for survivors of childhood cancers. Pediatr Blood Cancer 2014;61:1074–9. https://doi.org/10.1002/pbc.24947.
[76] Gunther JR, Sato M, Chintagumpala M, Ketonen L, Jones JY, Allen PK, et al. Imaging changes in pediatric intracranial ependymoma patients treated with proton beam radiation therapy compared to intensity modulated radiation therapy. Int J Radiat Oncol 2015;93:54–63. https://doi.org/10.1016/j.ijrobp.2015.05.018.
[77] Paganetti H, Niemierko A, Ancukiewicz M, Gerweck LE, Goitein M, Loeffler JS, et al. Relative biological effectiveness (RBE) values for proton beam therapy. Int J Radiat Oncol Biol Phys 2002;53:407–21.
[78] Bojaxhiu B, Ahlhelm F, Walser M, Placidi L, Kliebsch U, Mikroutsikos L, et al. Radiation necrosis and white matter lesions in pediatric patients with brain tumors treated with pencil beam scanning proton therapy. Int J Radiat Oncol Biol Phys 2018;100:987–96. https://doi.org/10.1016/j.ijrobp.2017.11.037.
[79] Gouw AA, Seewann A, Van Der Flier WM, Barkhof F, Rozemuller AM, Scheltens P, et al. Heterogeneity of small vessel disease: a systematic review of MRI and histopathology correlations. J Neurol Neurosurg Psychiatry 2011;82:126–35. https://doi.org/10.1136/jnnp.2009.204685.
[80] Kim KW, MacFall JR, Payne ME. Classification of white matter lesions on magnetic resonance imaging in elderly persons. Biol Psychiatry 2008;64:273–80. https://doi.org/10.1016/j.biopsych.2008.03.024.
[81] Wassenberg MWM, Bromberg JEC, Witkamp TD, Terhaard CHJ, Taphoorn MJB. White matter lesions and encephalopathy in patients treated for primary central nervous system lymphoma. 52. 2001. doi:https://doi.org/10.1023/A:1010676807228.
[82] Pantoni L. Cerebral small vessel disease: from pathogenesis and clinical characteristics to therapeutic challenges. Lancet Neurol 2010;9:689–701. https://doi.org/10.1016/S1474-4422(10)70104-6.
[83] Packer RJ, Zimmerman RA, Bilaniuk LT. Magnetic resonance imaging in the evaluation of treatment-related central nervous system damage. Cancer 1986;58:635–40. https://doi.org/10.1002/1097-0142(19860801)58:3<635::AID-CNCR2820580307>3.0.CO;2-X.
[84] Perry A, Schmidt RE. Cancer therapy-associated CNS neuropathology: An update and review of the literature. Acta Neuropathol 2006;111:197–212. https://doi.org/10.1007/s00401-005-0023-y.
[85] Pružincová L, Šteňo J, Srbecký M, Kalina P, Rychlý B, Bolješíková E, et al. MR imaging of late radiation therapy- and chemotherapy-induced injury: a pictorial essay. Eur Radiol 2009;19:2716–27. https://doi.org/10.1007/s00330-009-1449-8.
[86] Haris M, Kumar S, Raj MK, Das KJM, Sapru S, Behari S, et al. Serial diffusion tensor imaging to characterize radiation-induced changes in normal-appearing white matter following radiotherapy in patients with adult low-grade gliomas. Radiat Med – Med Imaging Radiat Oncol 2008;26:140–50. https://doi.org/10.1007/s11604-007-0209-4.
[87] Monaco EA, Faraji AH, Berkowitz O, Parry PV, Hadelsberg U, Kano H, et al. Leukoencephalopathy after whole-brain radiation therapy plus radiosurgery versus radiosurgery alone for metastatic lung cancer. Cancer 2013;119:226–32. https://doi.org/10.1002/cncr.27504.
[88] Swennen MHJ, Bromberg JEC, Witkamp TD, Terhaard CHJ, Postma TJ, Taphoorn MJB. Delayed radiation toxicity after focal or whole brain radiotherapy for low-grade glioma. J Neurooncol 2004;66:333–9. https://doi.org/10.1023/B:NEON.0000014518.16481.7e.
[89] Stokes TB, Niranjan A, Kano H, Choi PA, Kondziolka D, Dade Lunsford L, et al. White matter changes in breast cancer brain metastases patients who undergo radiosurgery alone compared to whole brain radiation therapy plus radiosurgery. J Neurooncol 2015;121:583–90. https://doi.org/10.1007/s11060-014-1670-4.
[90] Wardlaw JM, Smith EE, Biessels GJ, Cordonnier C, Fazekas F, Frayne R, et al. Neuroimaging standards for research into small vessel disease and its contribution to ageing and neurodegeneration. Lancet Neurol 2013;12:822–38. https://doi.org/10.1016/S1474-4422(13)70124-8.
[91] Østergaard L, Jespersen SN, Engedahl T, Jiménez EG, Ashkanian M, Hansen MB, et al. Capillary dysfunction: its detection and causative role in dementias and stroke. Curr Neurol Neurosci Rep 2015;15:37. https://doi.org/10.1007/s11910-015-0557-x.
[92] Fouladi M, Langston J, Mulhern R, Jones D, Xiong X, Yang J, et al. Silent lacunar lesions detected by magnetic resonance imaging of children with brain tumors: a late sequela of therapy. J Clin Oncol 2000;18:824–31. https://doi.org/10.1200/JCO.2000.18.4.824.
[93] Benjamin P, Trippier S, Lawrence AJ, Lambert C, Zeestraten E, Williams OA, et al. Lacunar infarcts, but not perivascular spaces, are predictors of cognitive decline in cerebral small-vessel disease. Stroke 2018;49:586–93. https://doi.org/10.1161/STROKEAHA.117.017526.
[94] Murphy ES, Xie H, Merchant TE, Yu JS, Chao ST, Suh JH. Review of cranial radiotherapy-induced vasculopathy. J Neurooncol 2015;122:421–9. https://doi.org/10.1007/s11060-015-1732-2.
[95] Barisano G, Bergamaschi S, Acharya J, Rajamohan A, Gibbs W, Kim P, et al. Complications of radiotherapy and radiosurgery in the brain and spine. Neurographics 2018;8:167–87. https://doi.org/10.3174/ng.1700066.
[96] Acharya S, Robinson CG, Michalski JM, Mullen D, DeWees TA, Campian JL, et al. Association of 1p/19q codeletion and radiation necrosis in adult cranial gliomas after proton or photon therapy. Int J Radiat Oncol Biol Phys 2018;101:334–43. https://doi.org/10.1016/j.ijrobp.2018.01.099.
[97] Kralik SF, Ho CY, Finke W, Buchsbaum JC, Haskins CP, Shih CS. Radiation necrosis in pediatric patients with brain tumors treated with proton radiotherapy. Am J Neuroradiol 2015;36:1572–8. https://doi.org/10.3174/ajnr.A4333.
[98] Fink J, Born D, Chamberlain MC. Radiation necrosis: Relevance with respect to treatment of primary and secondary brain tumors. Curr Neurol Neurosci Rep 2012;12:276–85. https://doi.org/10.1007/s11910-012-0258-7.
[99] Feng R, Loewenstern J, Aggarwal A, Pawha P, Gilani A, Iloreta AM, et al. Cerebral radiation necrosis: an analysis of clinical and quantitative imaging and volumetric features. World Neurosurg 2018;111:e485–94. https://doi.org/10.1016/j.wneu.2017.12.104.
[100] Zadeh MRN, Chapman CH, Chenevert T, Lawrence TS, Ten Haken RK, Tsien CI, et al. Response-driven imaging biomarkers for predicting radiation necrosis of the brain. Phys Med Biol 2014;59:2535–47. https://doi.org/10.1088/0031-9155/59/10/2535.
[101] Lawrence YR, Li XA, el Naqa I, Hahn CA, Marks LB, Merchant TE, et al. Radiation dose-volume effects in the brain. Int J Radiat Oncol Biol Phys 2010;76:S20–7. https://doi.org/10.1016/j.ijrobp.2009.02.091.
[102] Chao ST, Ahluwalia MS, Barnett GH, Stevens GHJ, Murphy ES, Stockham AL, et al. Challenges with the diagnosis and treatment of cerebral radiation necrosis. Int J Radiat Oncol Biol Phys 2013;87:449–57. https://doi.org/10.1016/j.ijrobp.2013.05.015.
[103] van Dijken BRJ, van Laar PJ, Holtman GA, van der Hoorn A. Diagnostic accuracy of magnetic resonance imaging techniques for treatment response evaluation in patients with high-grade glioma, a systematic review and meta-analysis. Eur Radiol 2017;27:4129–44. https://doi.org/10.1007/s00330-017-4789-9.
[104] Mittal S, Wu Z, Neelavalli J, Haacke EM. Susceptibility-weighted imaging: Technical aspects and clinical applications, Part 2. Am J Neuroradiol 2009;30:232–52. https://doi.org/10.3174/ajnr.A1461.
[105] Sehgal V, Delproposto Z, Haacke EM, Tong KA, Wycliffe N, Kido DK, et al. Clinical applications of neuroimaging with susceptibility-weighted imaging. J Magn Reson Imaging 2005;22:439–50. https://doi.org/10.1002/jmri.20404.
[106] Liu J, Xia S, Hanks R, Wiseman N, Peng C, Zhou S, et al. Susceptibility weighted imaging and mapping of micro-hemorrhages and major deep veins after traumatic brain injury. J Neurotrauma 2016;33:10–21. https://doi.org/10.1089/neu.2014.3856.
[107] Cheng AL, Batool S, McCreary CR, Lauzon ML, Frayne R, Goyal M, et al. Susceptibility-weighted imaging is more reliable than T2*-weighted

gradient-recalled echo MRI for detecting microbleeds. Stroke 2013;44:2782–6. https://doi.org/10.1161/STROKEAHA.113.002267.
[108] Nandigam RNK, Viswanathan A, Delgado P, Skehan ME, Smith EE, Rosand J, et al. MR imaging detection of cerebral microbleeds: effect of susceptibility-weighted imaging, section thickness, and field strength. Am J Neuroradiol 2009;30:338–43. https://doi.org/10.3174/ajnr.A1355.
[109] Goos JDC, Van Der Flier WM, Knol DL, Pouwels PJW, Scheltens P, Barkhof F, et al. Clinical relevance of improved microbleed detection by susceptibility-weighted magnetic resonance imaging. Stroke 2011;42:1894–900. https://doi.org/10.1161/STROKEAHA.110.599837.
[110] Vernooij MW, Ikram MA, Wielopolski PA, Krestin GP, Breteler M, van der Lugt A. Cerebral microbleeds: accelerated 3D T2*-weighted GRE MR imaging versus conventional 2D T2*-weighted GRE MR imaging for detection. Radiology 2008;248:272–7. https://doi.org/10.1148/radiol.2481071158.
[111] Bian W, Hess CP, Chang SM, Nelson SJ, Lupo JM. Susceptibility-weighted MR imaging of radiation therapy-induced cerebral microbleeds in patients with glioma: a comparison between 3T and 7T. Neuroradiology 2014;56:91–6. https://doi.org/10.1007/s00234-013-1297-8.
[112] Theysohn JM, Kraff O, Maderwald S, Barth M, Ladd SC, Forsting M, et al. 7 Tesla MRI of microbleeds and white matter lesions as seen in vascular dementia. J Magn Reson Imaging 2011;33:782–91. https://doi.org/10.1002/jmri.22513.
[113] Conijn MMA, Geerlings MI, Biessels GJ, Takahara T, Witkamp TD, Zwanenburg JJM, et al. Cerebral microbleeds on MR imaging: comparison between 1.5 and 7T. Am J Neuroradiol 2011;32:1043–9. https://doi.org/10.3174/ajnr.A2450.
[114] Hu R, Daftari Besheli L, Young J, Wu M, Pomerantz S, Lev MH, et al. Dual-energy head CT enables accurate distinction of intraparenchymal hemorrhage from calcification in emergency department patients. Radiology 2016;280:177–83. https://doi.org/10.1148/radiol.2015150877.
[115] Liu T, Surapaneni K, Lou M, Cheng L, Spincemaille P, Wang Y. Cerebral microbleeds: burden assessment by using quantitative susceptibility mapping. Radiology 2012;262:269–78. https://doi.org/10.1148/radiol.11110251.
[116] Ghassaban K, Liu S, Jiang C, Haacke EM. Quantifying iron content in magnetic resonance imaging. Neuroimage 2018:1–16. https://doi.org/10.1016/j.neuroimage.2018.04.047.
[117] Klohs J, Deistung A, Schweser F, Grandjean J, Dominietto M, Waschkies C, et al. Detection of cerebral microbleeds with quantitative susceptibility mapping in the ArcAbeta mouse model of cerebral amyloidosis. J Cereb Blood Flow Metab 2011;31:2282–92. https://doi.org/10.1038/jcbfm.2011.118.
[118] Kim SG, Harel N, Jin T, Kim T, Lee P, Zhao F. Cerebral blood volume MRI with intravascular superparamagnetic iron oxide nanoparticles. NMR Biomed 2013;26:949–62. https://doi.org/10.1002/nbm.2885.
[119] Han SH, Cho JH, Jung HS, Suh JY, Kim JK, Kim YR, et al. Robust MR assessment of cerebral blood volume and mean vessel size using SPION-enhanced ultrashort echo acquisition. Neuroimage 2015;112:382–9. https://doi.org/10.1016/j.neuroimage.2015.03.042.
[120] Girard OM, Ramirez R, Mccarty S, Mattrey RF. Toward absolute quantification of iron oxide nanoparticles as well as cell internalized fraction using multiparametric MRI. Contrast Media Mol Imaging 2012;7:411–7. https://doi.org/10.1002/cmmi.1467.
[121] Gambarota G, Van Laarhoven HWM, Philippens M, Lok J, Van Der Kogel A, Punt CJA, et al. Assessment of absolute blood volume in carcinoma by USPIO contrast-enhanced MRI. Magn Reson Imaging 2006;24:279–86. https://doi.org/10.1016/j.mri.2005.12.003.
[122] Nakagawa D, Kudo K, Awe O, Zanaty M, Nagahama Y, Cushing C, et al. Detection of microbleeds associated with sentinel headache using MRI quantitative susceptibility mapping: pilot study. J Neurosurg 2018:1–7. https://doi.org/10.3171/2018.2.JNS1884.
[123] Nakagawa D, Cushing C, Nagahama Y, Allan L, Hasan D. Quantitative susceptibility mapping as a possible tool to radiographically diagnose sentinel headache associated with intracranial aneurysm: case report. World Neurosurg 2017;103:954.e1–4. https://doi.org/10.1016/j.wneu.2017.04.151.
[124] Tan H, Zhang L, Mikati AG, Girard R, Khanna O, Fam MD, et al. Quantitative susceptibility mapping in cerebral cavernous malformations: clinical correlations. Am J Neuroradiol 2016;37:1209–15. https://doi.org/10.3174/ajnr.A4724.
[125] Tan H, Liu T, Wu Y, Thacker J, Shenkar R, Mikati AG, et al. Evaluation of iron content in human cerebral cavernous malformation using quantitative susceptibility mapping. Invest Radiol 2014;49:498–504. https://doi.org/10.1097/RLI.0000000000000043.
[126] Mikati AG, Tan H, Shenkar R, Li L, Zhang L, Guo X, et al. Dynamic permeability and quantitative susceptibility related imaging biomarkers in cerebral cavernous malformations. Stroke 2014;45:598–601. https://doi.org/10.1161/STROKEAHA.113.003548.
[127] Deh K, Nguyen TD, Eskreis-Winkler S, Prince MR, Spincemaille P, Gauthier S, et al. Reproducibility of quantitative susceptibility mapping in the brain at two field strengths from two vendors. J Magn Reson Imaging 2015;42:1592–600. https://doi.org/10.1002/jmri.24943.
[128] Khong PL, Kwong DLW, Chan GCF, Sham JST, Chan FL, Ooi GC. Diffusion-tensor imaging for the detection and quantification of treatment-induced white matter injury in children with medulloblastoma: a pilot study. Am J Neuroradiol 2003;24:734–40.
[129] Brinkman TM, Reddick WE, Luxton J, Glass JO, Sabin ND, Srivastava DK, et al. Cerebral white matter integrity and executive function in adult survivors of childhood medulloblastoma. Neuro Oncol 2012;14:iv5–iv26. https://doi.org/10.1093/neuonc/nos214.
[130] Aukema EJ, Caan MWA, Oudhuis N, Majoie CBLM, Vos FM, Reneman L, et al. White matter fractional anisotropy correlates with speed of processing and motor speed in young childhood cancer survivors. Int J Radiat Oncol Biol Phys 2009;74:837–43. https://doi.org/10.1016/j.ijrobp.2008.08.060.
[131] King TZ, Wang L, Mao H. Disruption of white matter integrity in adult survivors of childhood brain tumors: Correlates with long-term intellectual outcomes. PLoS One 2015;10:1–17. https://doi.org/10.1371/journal.pone.0131744.
[132] Chapman CH, Nagesh V, Sundgren PC, Buchtel H, Chenevert TL, Junck L, et al. Diffusion tensor imaging of normal-appearing white matter as biomarker for radiation-induced late delayed cognitive decline. Int J Radiat Oncol Biol Phys 2012;82:2033–40. https://doi.org/10.1016/j.ijrobp.2011.01.068.
[133] Khong PL, Leung LHT, Fung ASM, Fong DYT, Qiu D, Kwong DLW, et al. White matter anisotropy in post-treatment childhood cancer survivors: preliminary evidence of association with neurocognitive function. J Clin Oncol 2006;24:884–90. https://doi.org/10.1200/JCO.2005.02.4505.
[134] Chapman CH, Zhu T, Nazem-Zadeh M, Tao Y, Buchtel HA, Tsien CI, et al. Diffusion tensor imaging predicts cognitive function change following partial brain radiotherapy for low-grade and benign tumors. Radiother Oncol 2016;120:234–40. https://doi.org/10.1016/j.radonc.2016.06.021.
[135] Ravn S, Holmberg M, Sorensen P, Frokjær JB, Carl J. Differences in supratentorial white matter diffusion after radiotherapy-new biomarker of normal brain tissue damage? Acta Oncol (Madr) 2013;52:1314–9. https://doi.org/10.3109/0284186X.2013.812797.
[136] Nagesh V, Tsien CI, Chenevert TL, Ross BD, Lawrence TS, Junick L, et al. Radiation-induced changes in normal-appearing white matter in patients with cerebral tumors: a diffusion tensor imaging study. Int J Radiat Oncol Biol Phys 2008;70:1002–10. https://doi.org/10.1016/j.ijrobp.2007.08.020.
[137] Ding Z, Zhang H, Lv XF, Xie F, Liu L, Qiu S, et al. Radiation-induced brain structural and functional abnormalities in presymptomatic phase and outcome prediction. Hum Brain Mapp 2018;39:407–27. https://doi.org/10.1002/hbm.23852.
[138] Mouridsen K, Hansen MB, Østergaard L, Jespersen SN. Reliable estimation of capillary transit time distributions using DSC-MRI. J Cereb Blood Flow Metab 2014;34:1511–21. https://doi.org/10.1038/jcbfm.2014.111.
[139] Hansen MB, Tietze A, Kalpathy-Cramer J, Gerstner ER, Batchelor TT, Østergaard L, et al. Reliable estimation of microvascular flow patterns in patients with disrupted blood–brain barrier using dynamic susceptibility contrast MRI. J Magn Reson Imaging 2017;46:537–49. https://doi.org/10.1002/jmri.25549.
[140] Østergaard L, Engedal TS, Moreton F, Hansen MB, Wardlaw JM, Dalkara T, et al. Cerebral small vessel disease: Capillary pathways to stroke and cognitive decline. J Cereb Blood Flow Metab 2016;36:302–25. https://doi.org/10.1177/0271678X15606723.
[141] Engedal TS, Hjort N, Hougaard KD, Simonsen CZ, Andersen G, Mikkelsen IK, et al. Transit time homogenization in ischemic stroke – a novel biomarker of penumbral microvascular failure? J Cereb Blood Flow Metab 2018;38:2006–20. https://doi.org/10.1177/0271678X17721666.
[142] Emblem KE, Farrar CT, Gerstner ER, Batchelor TT, Borra RJH, Rosen BR, et al. Vessel caliber–a potential MRI biomarker of tumour response in clinical trials. Nat Rev Clin Oncol 2014;11:566–84. https://doi.org/10.1038/nrclinonc.2014.126.
[143] Stadlbauer A, Zimmermann M, Kitzwögerer M, Oberndorfer S, Rössler K, Dörfler A, et al. MR imaging-derived oxygen metabolism and neovascularization characterization for grading and idh gene mutation detection of gliomas. Radiology 2017;283:799–809. https://doi.org/10.1148/radiol.2016161422.
[144] Kang HY, Xiao HL, Chen JH, Tan Y, Chen X, Xie T, et al. Comparison of the effect of vessel size imaging and cerebral blood volume derived from perfusion MR imaging on glioma grading. Am J Neuroradiol 2016;37:51–7. https://doi.org/10.3174/ajnr.A4477.
[145] Macdonald ME, Frayne R. Cerebrovascular MRI: a review of state-of-the-art approaches, methods and techniques. NMR Biomed 2015;28:767–91. https://doi.org/10.1002/nbm.3322.
[146] Petr J, Platzek I, Seidlitz A, Mutsaerts HJMM, Hofheinz F, Schramm G, et al. Early and late effects of radiochemotherapy on cerebral blood flow in glioblastoma patients measured with non-invasive perfusion MRI. Radiother Oncol 2016;118:24–8. https://doi.org/10.1016/j.radonc.2015.12.017.
[147] Jakubovic R, Sahgal A, Ruschin M, Pejović-Milić A, Milwid R, Aviv RI. Non tumor perfusion changes following stereotactic radiosurgery to brain metastases. Technol Cancer Res Treat 2015;14:497–503. https://doi.org/10.1177/1533034614600279.
[148] Cebeci H, Aydin O, Ozturk-Isik E, Gumus C, Inecikli F, Bekar A, et al. Assesment of perfusion in glial tumors with arterial spin labeling; comparison with dynamic susceptibility contrast method. Eur J Radiol 2014;83:1914–9. https://doi.org/10.1016/j.ejrad.2014.07.002.
[149] Warmuth C, Günther M, Zimmer C. Quantification of blood flow in brain tumors: comparison of arterial spin labeling and dynamic susceptibility-weighted contrast-enhanced MR imaging. Radiology 2003;228:523–32. https://doi.org/10.1148/radiol.2282020409.
[150] Noguchi T, Yoshiura T, Hiwatashi A, Togao O, Yamashita K, Nagao E, et al. Perfusion imaging of brain tumors using arterial spin-labeling: correlation with histopathologic vascular density. Am J Neuroradiol 2008;29:688–93. https://doi.org/10.3174/ajnr.A0903.

[151] Le Bihan D, Breton E, Lallemand D, Grenier P, Cabanis E, Laval-Jeantet M. MR imaging of intravoxel incoherent motions: application to diffusion and perfusion in neurologic disorders. Radiology 1986;161:401–7. https://doi.org/10.1148/radiology.161.2.3763909.

[152] Federau C, O'Brien K, Meuli R, Hagmann P, Maeder P. Measuring brain perfusion with intravoxel incoherent motion (IVIM): Initial clinical experience. J Magn Reson Imaging 2014;39:624–32. https://doi.org/10.1002/jmri.24195.

[153] Shen N, Zhao L, Jiang J, Jiang R, Su C, Zhang S, et al. Intravoxel incoherent motion diffusion-weighted imaging analysis of diffusion and microperfusion in grading gliomas and comparison with arterial spin labeling for evaluation of tumor perfusion. J Magn Reson Imaging 2016;44:620–32. https://doi.org/10.1002/jmri.25191.

[154] Zhang X, Ingo C, Teeuwisse WM, Chen Z, van Osch MJP. Comparison of perfusion signal acquired by arterial spin labeling–prepared intravoxel incoherent motion (IVIM) MRI and conventional IVIM MRI to unravel the origin of the IVIM signal. Magn Reson Med 2018;79:723–9. https://doi.org/10.1002/mrm.26723.

[155] Wong SM, Zhang CE, van Bussel FCG, Staals J, Jeukens CRLPN, Hofman PAM, et al. Simultaneous investigation of microvasculature and parenchyma in cerebral small vessel disease using intravoxel incoherent motion imaging. NeuroImage Clin 2017;14:216–21. https://doi.org/10.1016/j.nicl.2017.01.017.

[156] Shih HA, Sherman JC, Nachtigall LB, Colvin MK, Fullerton BC, Daartz J, et al. Proton therapy for low-grade gliomas: Results from a prospective trial. Cancer 2015;121:1712–9. https://doi.org/10.1002/cncr.29237.